



Frequent homozygous deletion of *Cdkn2a/2b* in tremolite-induced malignant mesothelioma in rats

Yasumasa Okazaki¹  | Nobuaki Misawa¹ | Shinya Akatsuka¹ | Norihiko Kohyama^{2,3} | Yoshitaka Sekido⁴ | Takashi Takahashi^{5,6} | Shinya Toyokuni¹ 

¹Department of Pathology and Biological Responses, Nagoya University Graduate School of Medicine, Nagoya, Japan

²Faculty of Economics, Toyo University Graduate School of Economics, Tokyo, Japan

³National Institute of Occupational Safety and Health, Kawasaki, Japan

⁴Division of Cancer Biology, Aichi Cancer Center Research Institute, Nagoya, Japan

⁵Division of Molecular Carcinogenesis, Nagoya University Graduate School of Medicine, Nagoya, Japan

⁶Aichi Cancer Center Research Institute, Nagoya, Japan

Correspondence

Shinya Toyokuni and Yasumasa Okazaki, Department of Pathology and Biological Responses, Nagoya University Graduate School of Medicine, 65 Tsurumai-cho, Showa-ku, Nagoya, Aichi 466-8550, Japan. Emails: toyokuni@med.nagoya-u.ac.jp (ST); samasuya@med.nagoya-u.ac.jp (YO)

Funding information

Japan Society for the Promotion of Science, Grant/Award Number: JP17H04064 and JP19H05462 and JP25860292

Abstract

The onset of malignant mesothelioma (MM) is linked to exposure to asbestos fibers. Asbestos fibers are classified as serpentine (chrysotile) or amphibole, which includes the crocidolite, amosite, anthophyllite, tremolite, and actinolite types. Although few studies have been undertaken, anthophyllite has been shown to be associated with mesothelioma, and tremolite, a contaminant in talc and chrysotile, is a risk factor for carcinogenicity. Here, after characterizing the length and width of these fibers by scanning electron microscopy, we explored the cytotoxicity induced by tremolite and anthophyllite in cells from an immortalized human mesothelial cell line (MeT5A), murine macrophages (RAW264.7), and in a rat model. Tremolite and short anthophyllite fibers were phagocytosed and localized to vacuoles, whereas the long anthophyllite fibers were caught on the pseudopod of the MeT5A and Raw 264.7 cells, according to transmission electron microscopy. The results from a 2-day time-lapse study revealed that tremolite was engulfed and damaged the MeT5A and RAW264.7 cells, but anthophyllite was not cytotoxic to these cells. Intraperitoneal injection of tremolite in rats induced diffuse serosal thickening, whereas anthophyllite formed focal fibrosis and granulomas on peritoneal serosal surfaces. Furthermore, the loss of *Cdkn2a/2b*, which are the most frequently lost foci in human MM, were observed in 8 cases of rat MM (homozygous deletion [5/8] and loss of heterozygosity [3/8]) by array-based comparative genomic hybridization techniques. These results indicate that tremolite initiates mesothelial injury and persistently frustrates phagocytes, causing subsequent peritoneal fibrosis and MM. The possible mechanisms of carcinogenicity based on fiber diameter/length are discussed.

KEYWORDS

animal model, anthophyllite, *Cdkn2a/2b*, malignant mesothelioma, tremolite

1 | INTRODUCTION

Asbestos, which are naturally occurring fibrous minerals, are classified as carcinogens on the basis of sufficient evidence in

humans; thus, many countries have banned the use of all asbestos.¹ The WHO estimates that more than 107 000 people die each year from asbestos-related lung cancer, malignant mesothelioma (MM), and asbestosis from occupational exposure.² Malignant

This is an open access article under the terms of the Creative Commons Attribution-NonCommercial License, which permits use, distribution and reproduction in any medium, provided the original work is properly cited and is not used for commercial purposes.

© 2020 The Authors. *Cancer Science* published by John Wiley & Sons Australia, Ltd on behalf of Japanese Cancer Association.

mesothelioma arises from mesothelial cells, which line somatic cavities, such as the pleural cavity, peritoneal cavity, pericardial cavity, and tunica vaginalis, and is one of the most lethal neoplasms in humans.³

The asbestos fiber is defined by its chemical components and length/diameter ratio; the length is more than 3 times greater than the diameter and longer than 5 μm .⁴ The crystal structure of asbestos grows in 2 or 3 dimensions and is cleaved into fragments or broken into fibrils. Amosite, chrysotile, and crocidolite are present in the asbestiform habit, whereas tremolite, actinolite, and anthophyllite are present in either the asbestiform or nonasbestiform habits.⁴ Tremolite is a relatively common contaminant in chrysotile and talc deposits because the constitutional elements of asbestos fibers are similar. Actinolite is a common contaminant in amosite and is known as an iron-substituted derivative of tremolite. Anthophyllite is relatively rare and is occasionally found as a contaminant in talc deposits.⁴ Although some talc products are contaminated with these types of asbestos, the association between the mesothelioma and talc exposure remains controversial.^{5,6}

Anthophyllite has been mined in small quantities around the world, most notably in Finland; hence, anthophyllite is the most common amphibole found in the lung of the Finnish population.⁷ The environmental exposure of anthophyllite induces focal pleural plaque with calcification, but not diffuse pleural thickening or MM, in Finland and Japan.⁸ Anthophyllite fibers are generally coarser and longer than those of the other amphiboles; thus, it is postulated that anthophyllite is a less potent carcinogen.⁹⁻¹¹ In contrast, the higher biodegradability of anthophyllite, which is as high as that of crocidolite, is speculated to exacerbate the higher carcinogenicity than chrysotile.¹² Indeed, the workers at anthophyllite quarries¹¹ and a Finnish teacher who did not have a history of occupational asbestos exposure⁷ developed MM, and their lungs were burdened with anthophyllite but not the other asbestos fibers. Although these human data have led to the assessment of carcinogenicity for anthophyllite, the estimation of the potential risk is difficult to determine from an epidemiological standpoint, as anthophyllite is sometimes found as a contaminant of other asbestos or talc deposits.⁹ However, the inhalation of tremolite, which is a contaminant in chrysotile, induced stronger pulmonary fibrosis than pure chrysotile, according to an epidemiological chest X-ray study.¹³ Recently, a former worker in a quarry where hornblende gabbro, but not asbestos, was mined in Japan, developed lung cancer with a massive burden of tremolite fibers.¹⁴ Therefore, the risk of carcinogenicity of tremolite is of great concern.

Excellent durability of asbestos fibers causes continuous stimulation and initiates mesothelial injury and frustrated phagocytosis in the tissue surrounding the fibers.^{3,15} The internalized asbestos fibers produce cytotoxic reactive oxygen species (ROS) and are presumed to cause chromosomal tangling during mitosis and to accelerate the cellular damage caused by the absorbed iron and carcinogens.^{3,16} Here, anthophyllite from Afghanistan, whose proportion of talc is much lower than the UICC standard anthophyllite from Finland¹⁷ and tremolite from Japan were used to explore

the asbestos-induced mesothelial injury. In this study, we found that tremolite caused cellular damage in MeT5A mesothelial and RAW264.7 macrophage cells, and diffuse peritoneal thickening and MM in rats; however, the long anthophyllite fiber was not cytotoxic. Using array-based comparative genomic hybridization (aCGH) techniques, we detected the frequent loss of *Cdkn2a/2b* in tremolite-induced MM in rats.

2 | MATERIALS AND METHODS

2.1 | Reagents

Cell counting reagent SF, based on water soluble tetrazolium salt-8 (WST-8), antibiotic-antimycotic mixed stock solution (100 \times ; stabilized), 0.5% trypan blue solution, RPMI-1640, DMEM, and nitrilotriacetic acid disodium salt were obtained from Nacalai Tesque. Medium 199 and GlutaMAX were purchased from Invitrogen Life Technologies. Glass-based dishes (35 mm) were obtained from AGC Techno Glass. Fetal bovine serum was obtained from BioWest. Cellmatrix (Type I-C) collagen was obtained from Nitta Gelatin. CytoTox-ONE homogeneous membrane integrity assay was obtained from Promega. Epidermal growth factor (EGF), hydrocortisone solution and lead stain solution were obtained from Sigma-Aldrich. Insulin was obtained from Roche Diagnostics. Trace element B was obtained from Mediatech. Paraformaldehyde, DMP-30, MNA, DDSA, and EPON812 resin were obtained from TAAB Laboratories Equipment. Osmium tetroxide, EM fine grid F-200, and a Veco grid (Au 300 mesh) were obtained from NISSHIN EM. Glutaraldehyde aqueous solution (practical grade) was obtained from Electron Microscopy Sciences. The DNeasy Blood & Tissue Kit was obtained from Qiagen. All the chemicals used in this study were of analytical quality from Wako. Crocidolite and chrysotile were from UICC. Anthophyllite and tremolite were obtained as previously described.^{17,18} These asbestos fibers were dispersed in physiological saline and sonicated (Astrason Ultrasonic Processor XL2020; Misonix Fisher Scientific) for 30 minutes.

2.2 | Cell cultures

MeT5A cells, an immortalized human mesothelial cell line, were maintained in M199 with FBS (10%), EGF (3.3 nM), insulin (860 nM), trace elements B, hydrocortisone (400 nM), and an antibiotic-antimycotic solution (1 \times). RAW264.7 murine macrophage and HeLa cells were maintained in DMEM with FBS (10%), GlutaMAX (1 \times), and an antibiotic-antimycotic solution (1 \times). MeT5A, RAW264.7, and HeLa cell lines were obtained from ATCC and 3 mesothelioma cell lines, named Meso8A, Meso8D, and Meso12A,¹⁹ were provided by Dr Yoshitaka Sekido (Division of Cancer Biology, Aichi Cancer Center) and maintained in RPMI-1640 with FBS (10%) and an antibiotic-antimycotic solution (1 \times). HeLa cells were used as the non-MM cancer cells with

which to compare the characteristics of the response of the immortalized mesothelial cells and MM cells against asbestos fibers.

2.3 | Scanning electron microscopy study

In brief, 0.1 μg tremolite and 1 μg anthophyllite were washed with Milli-Q water 3 times. These asbestos samples were dried in a 6-well plate and transferred onto carbon double-sided tape with brass setting. After coating with carbon, the samples were observed and the energy-dispersive X-ray spectrometer (EDS) analyses of the asbestos fibers were undertaken with a JSM-7610F scanning electron microscope (SEM; JEOL). The length and width of 300 asbestos fibers were determined based on a photomicrograph by cellSens software (Olympus).

2.4 | Transmission electron microscopy study

MeT5A and RAW264.7 cells were seeded at a density of 10 000 cells/ cm^2 in 6-well plates. After overnight incubation, anthophyllite, crocidolite, or tremolite (5 $\mu\text{g}/\text{cm}^2$) was added to each well and incubated for 3 hours. Then the cell pellets were harvested and fixed in fixative solution (2% paraformaldehyde, 2.5% glutaraldehyde in 0.1 M phosphate buffer, pH 7.4). After postfixing with osmium tetroxide, the samples were embedded in resin. After polymerization, the ultrathin sliced resins (80 nm) were stained with uranium acetate and lead solution. After staining, the samples were observed with a JEM-1400 PLUS microscope (JEOL). At the same time, the ultrathin sliced samples, which were stained neither with uranium nor lead, were analyzed with EDS using a gold grid.

2.5 | Time-lapse observation of uptake of asbestos fibers

Cells from 6 cell lines (MeT5A, RAW264.7, HeLa, Meso8A, Meso8D, and Meso12A) were seeded at a density of 2800 cells/ cm^2 in glass-based dishes. After overnight incubation, anthophyllite (5 $\mu\text{g}/\text{cm}^2$), tremolite (5 $\mu\text{g}/\text{cm}^2$), or saline was added to each dish and observed for 48 hours, using a LCV110 incubator microscope (Olympus). Images were generated as a video file with MetaMorph software (Molecular Devices Japan).

2.6 | Cell proliferation assay

Cell proliferation assays were carried out using WST-8 according to the manufacturer's protocol. In brief, cells from 6 cell lines were seeded at a density of 10 000 cells/ cm^2 in 96-well plates. After overnight incubation, 8 groups were prepared: anthophyllite (Ant) at 1, 5, and 10 $\mu\text{g}/\text{cm}^2$, tremolite (Tre) at 1, 5, and 10 $\mu\text{g}/\text{cm}^2$, crocidolite (Cro) at 10 $\mu\text{g}/\text{cm}^2$, and saline. The absorbance of the cells was measured on days 1, 2, and 3. For cell counting, cells from 6 cell lines

TABLE 1 Experimental groups of rats

Treatment	Female	Male
For assessment of fibrogenicity		
Saline	3	3
Saline + NTA	4	3
Chrysotile	2	2
Anthophyllite + saline	4	3
Anthophyllite + NTA	4	3
Tremolite + saline	4	3
Tremolite + NTA	4	3
For assessment of genomic alterations by array CGH		
Tremolite + saline	2	2
Tremolite + NTA	2	2

Abbreviations: CGH, comparative genome hybridization; NTA, nitrilotriacetic acid.

were seeded at a density of 5000 cells/ cm^2 in 24-well plates. Cells were trypsinized and counted with a hemocytometer on days 2, 4, and 6.

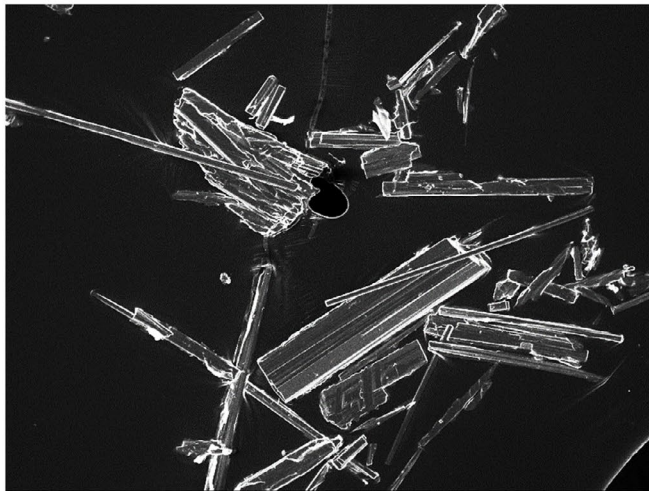
2.7 | Release of lactate dehydrogenase assay

Cultured cells were seeded at 10 000 cells/ cm^2 in clear-bottomed 96-well plates. After overnight incubation, 9 groups were prepared: Ant at 1, 5, and 10 $\mu\text{g}/\text{cm}^2$, Tre at 1, 5, and 10 $\mu\text{g}/\text{cm}^2$, Cro at 10 $\mu\text{g}/\text{cm}^2$, saline, and 100% cell lysis control (positive control used as a denominator). After incubation for 24 hours, the levels of lactate dehydrogenase (LDH) activity in media were measured according to the manufacturer's protocol in black 96-well plates. The data were corrected by the lysed samples and expressed as the percentage of the total intracellular LDH.

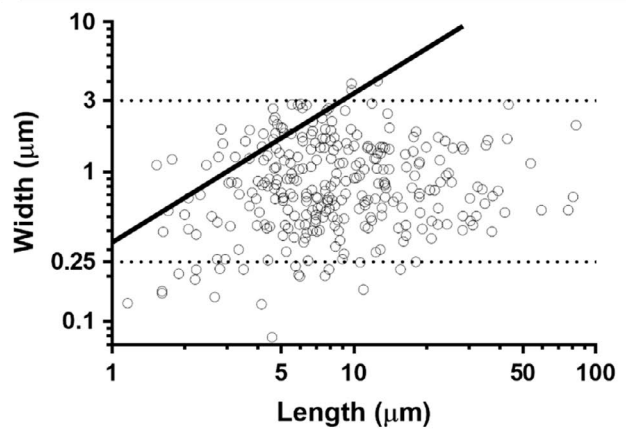
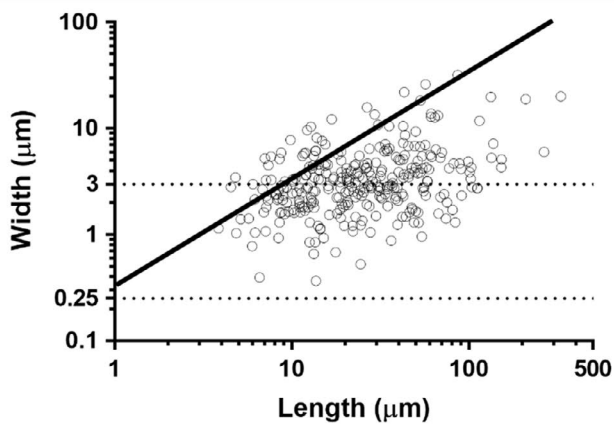
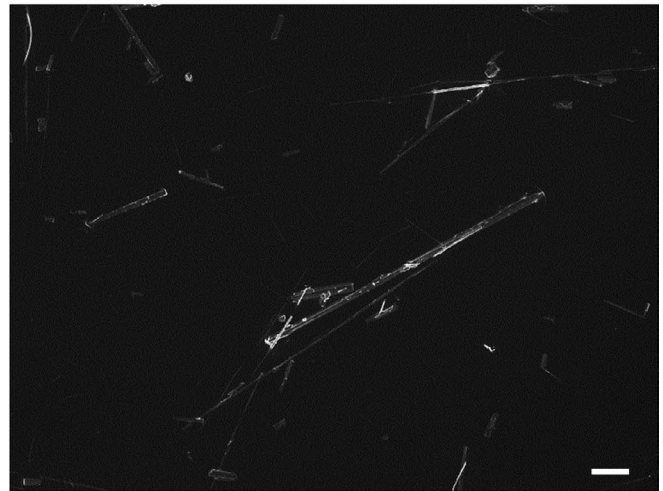
2.8 | Assessment of fibrogenicity of tremolite and anthophyllite in rats

The animal experiment committee of the Nagoya University Graduate School of Medicine approved the experiments undertaken in this study. Six-week-old F1 hybrid rats, the offspring of Fischer 344 and Brown Norway rats (Charles River Japan), were used in this study. The rats were maintained in a specific pathogen-free environment at 24°C with a 12:12-hour dark : light cycle. The rats were randomly divided into the following 7 groups: saline, nitrilotriacetate (NTA), chrysotile (Chry), Ant + NTA, Ant + saline, Tre + NTA, and Tre + saline (Table 1). At the 6th week, the rats were i.p. injected with saline or 1 mg asbestos (Chry, Ant, or Tre). Two weeks later, the rats were treated with either saline or NTA (80 mg/kg body weight) once a week for 2 weeks. After the rats were killed at the 10th week, macroscopic and microscopic examinations were carried out. For the assessment of fibrogenicity, the thickness of the liver surface was

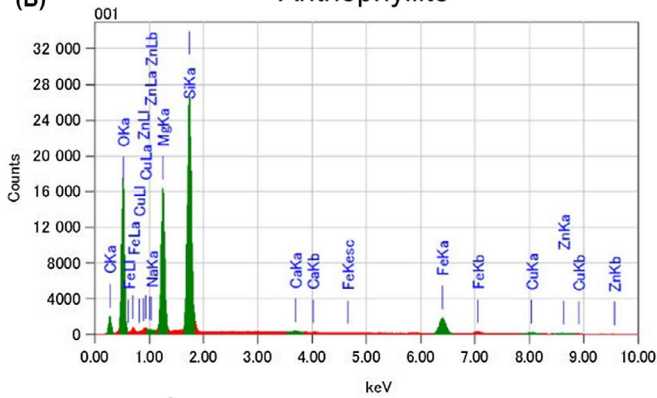
(A) Anthrophyllite



Tremolite



(B) Anthrophyllite



Tremolite

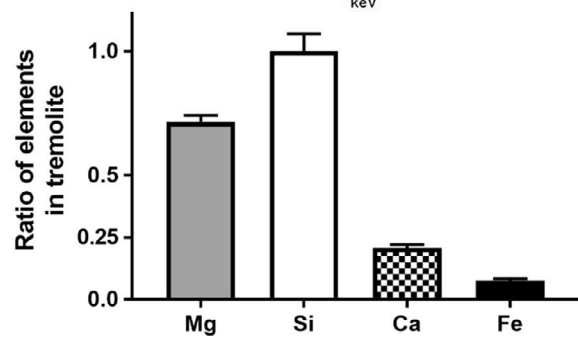
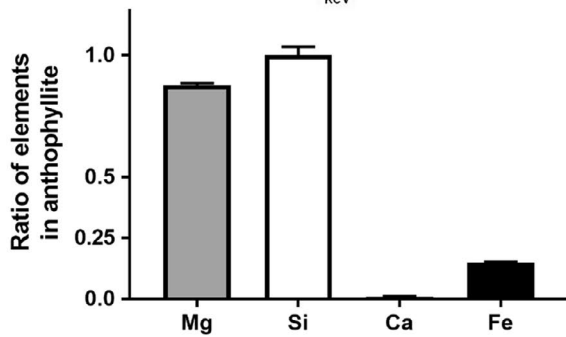
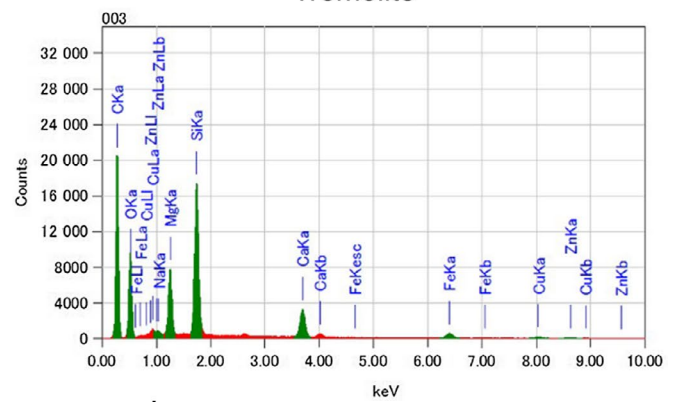


FIGURE 1 Measurements of width, length, and mineral content of anthophyllite and tremolite. A, Distributions of anthophyllite and tremolite by their width and length were determined by SEM. Representative photographs are shown. Anthophyllite is longer and thicker than tremolite, and the fraction of nonasbestiform was similar (anthophyllite, 9%; tremolite, 8.3%). Anthophyllite was approximately 3 times longer and 4 times thicker than tremolite (scale bar = 1 μm ; the aspect ratio 3 is shown as lines to indicate the boundary of the definition of asbestos). B, Analyses of the energy-dispersive X-ray spectrometer data revealed that the chemical formula of anthophyllite was $\text{Mg}_6\text{Fe}_1\text{Si}_8\text{O}_{22}(\text{OH})_2$ and the contamination of tremolite with actinolite was low. Cu and Zn was detected from the brass setting

determined at 10 random points, using a DMD108 light microscope (Leica Microsystems).

2.9 | Array-based comparative genomic hybridization analysis

The 8 cases of tremolite-induced peritoneal MM, which had been produced previously,¹⁸ were analyzed. Tremolite-induced MM frozen stock samples from our previous experiments were selected as follows: 2 male rats injected with either saline or NTA and 2 female rats injected with either saline or NTA (Table 1). Oligonucleotide microarrays for rat 4x180k CGH (G4826A), which were purchased from Agilent Technologies, were used in this study. In brief, 0.8 μg DNA was labeled, hybridized, and scanned according to the manufacturer's protocol. The scanned results were converted to \log_2 -transformed data and analyzed with the Agilent Genomic Workbench Standard Edition (version 5.0). To analyze the relationship between the genomic alterations of *Cdkn2a/2b* and rat lifespans, previously published aCGH data based on 12 cases of multiwalled carbon nanotube (MWCNT)-induced MM were used to supplement the MM cases.²⁰

2.10 | Statistical analysis

The data were analyzed using a paired *t* test and Fisher's exact test, and a difference was considered to be significant when *P* was less than .05. These analyses were undertaken using GraphPad Prism 7 Software (GraphPad Software).

3 | RESULTS

3.1 | Distinct physical dimensions of anthophyllite and tremolite fibers

The asbestiform, with an aspect ratio that is greater than 3, was 91% for the anthophyllite fiber and 92% for the tremolite fiber, as determined by SEM (Figure 1A). The median, mean, and standard deviation of the length and width of the anthophyllite and tremolite fibers are summarized in Table 2. Tremolite fibers (median length, 7.76 μm ; median diameter, 787 nm) were significantly thinner and shorter than anthophyllite fibers (median length, 23.55 μm ; median diameter, 2940 nm). The EDS analyses revealed the relative ratio of Mg, Si, Ca, and Fe in the asbestos fibers (Figure 1B). The anthophyllite was determined to be $\text{Mg}_6\text{Fe}_1\text{Si}_8\text{O}_{22}(\text{OH})_4$. The contamination level

of actinolite, which is also known as an iron-substituted tremolite, was not high in the tremolite sample ($\text{Ca}_2\text{Mg}_5\text{Si}_8\text{O}_{22}(\text{OH})_4$). These elemental analyses were confirmed with TEM-EDS (Figure S1A). The estimation of the elements in crocidolite was concordant with the ideal formula, $\text{Na}_2\text{Fe}_5\text{Si}_8\text{O}_{22}(\text{OH})_4$, indicating a good agreement between the acquired data and the estimation.

3.2 | MeT5A and RAW264.7 cells phagocytose short anthophyllite/tremolite fibers but not long anthophyllite fibers

Ultrathin sliced specimens for observation with transmission electron microscopy were broken off due to the presence of rigid asbestos fibers, which sometimes crushed the diamond knife. Both MeT5A and RAW264.7 cells phagocytosed short anthophyllite and tremolite fibers, which were transferred to phagosomes (Figure 2). In contrast, long anthophyllite fibers were attached to the pseudopod in MeT5A and RAW264.7 cells (Figure 2). Crocidolite fibers were also captured and translocated into phagosomes in MeT5A and RAW 264.7 cells (Figure S1B).

3.3 | Long anthophyllite fibers provide characteristic periodical movement with MeT5A and RAW264.7 cells

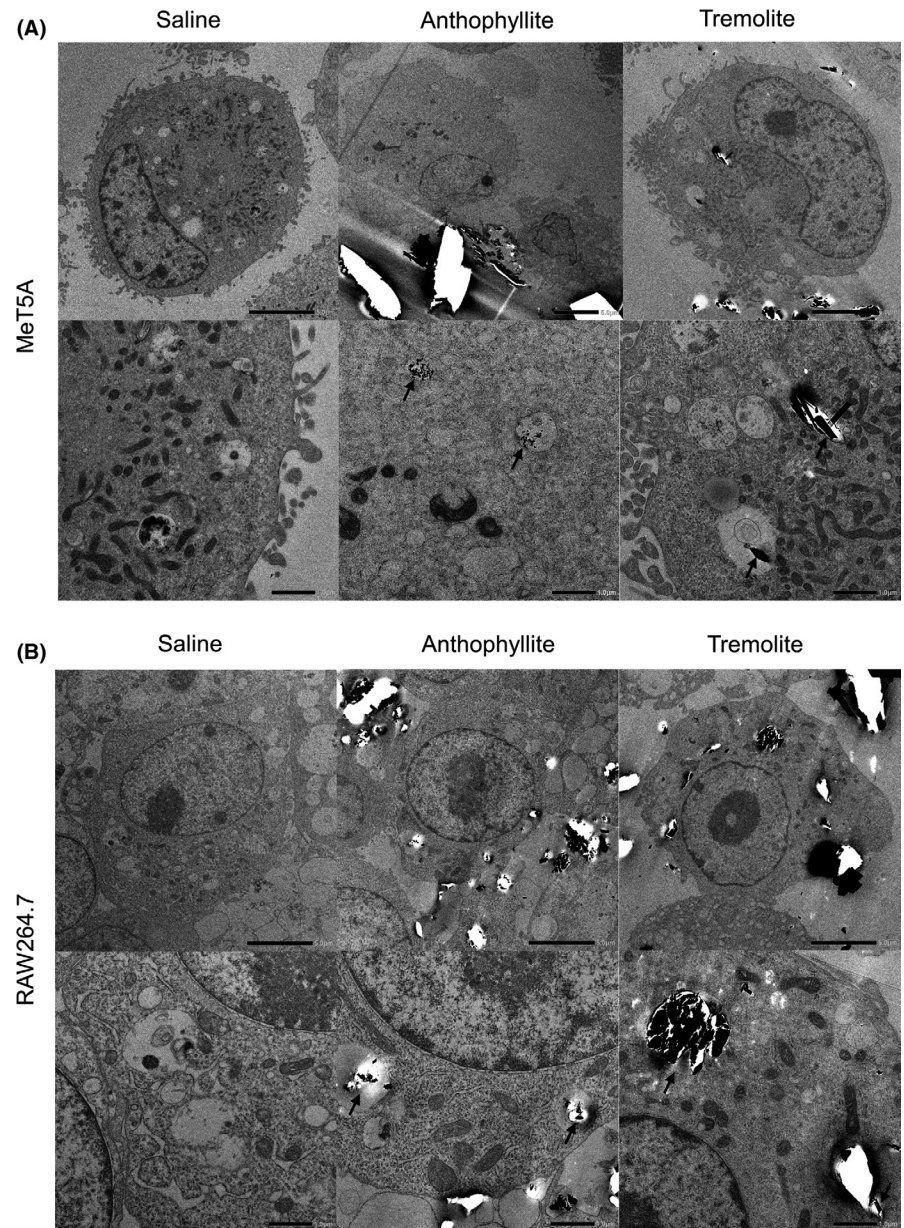
Long anthophyllite fibers were swung by contact with MeT5A cells (Figure 3A, Video S1) and were vibrated by contact with

TABLE 2 Length and width of anthophyllite and tremolite fibers used

	Anthophyllite		Tremolite	
Concentration of fibers	2.81×10^7 fibers/mg		11.76×10^7 fibers/mg	
Counted number of fibers	300		300	
	Length (μm)	Width (μm)	Length (μm)	Width (μm)
Median	23.55	2.94	7.76	0.787
Mean	34.27	4.06	11.42*	0.993*
Standard deviation	35.96	3.83	11.36	0.682

**P* < .001 vs anthophyllite.

FIGURE 2 Short anthophyllite and tremolite fibers are phagocytosed and localized in phagosomes, while long anthophyllite fibers attach to the plasma membrane of MeT5A and RAW264.7 cells, as observed by transmission electron microscopy. A, Large fibers of anthophyllite crushed the diamond knife; thus, only clefts were sometimes observed after ultrathin cutting. Short anthophyllite fibers were phagocytosed, whereas long ones were attached to the pseudopod of plasma membrane. Tremolite was observed in phagosomes more frequently and with fewer artificial clefts than anthophyllite, consistent with the short and thin dimensions of tremolite. B, Short anthophyllite fibers were phagocytosed. Pseudopods extended to catch anthophyllite fibers. Some bundles of tremolite fibers attached to the plasma membrane, and other tremolite fibers were observed in the phagosomes (arrows indicate internalized asbestos fibers)



RAW264.7 cells (Figure 3B, Video S2). Short anthophyllite and tremolite fibers were taken up into the cytoplasm and fixed like a floor cleaning mop within the MeT5A and RAW264.7 cells (Figure 3, Videos S1-S4). Contact with a long anthophyllite fiber promoted RAW264.7 cells to gather around the fiber. This cellular aggregation was not obvious with MeT5A cells nor the other cell lines (HeLa, Meso8A, and Meso8D), although all of them swung the long anthophyllite fiber (Figure S2, Videos S5-S7). RAW264.7 cells increased the volume after engulfing tremolite or short anthophyllite fibers (Figure 3B) whereas the Meso8A and Meso8D cells, which were established from the same MM patient,¹⁹ and the HeLa cells phagocytosed and held the tremolite and short anthophyllite fibers, as did the MeT5A cells (Figure S2, Videos S8-S10). The low frequency of swinging the long anthophyllite and internalization of the short anthophyllite and tremolite fibers was observed in Meso12A cells, presumably due

to the minimal cellular movements (Figure S2, Videos S11 and S12).

3.4 | Anthophyllite does not affect but tremolite suppresses the proliferation of MeT5A, RAW264.7, HeLa, Meso8A, Meso8D, and Meso12A cells

Anthophyllite exposure did not affect the proliferation of the MeT5A or RAW264.7 cells up to $10 \mu\text{g}/\text{cm}^2$ (Figure 4A-D). However, tremolite even at $1 \mu\text{g}/\text{cm}^2$ suppressed cellular proliferation, which was in a dose-dependent manner (Figure 4A-D). The cytotoxic effects in the MeT5A cells with high-dose exposure to tremolite were observed at early time points (Figure 4C). These cytotoxic effects of tremolite were also observed in the other cell lines used (Figures S3 and S4). Of note, only RAW264.7 cells were resistant to high-dose exposure

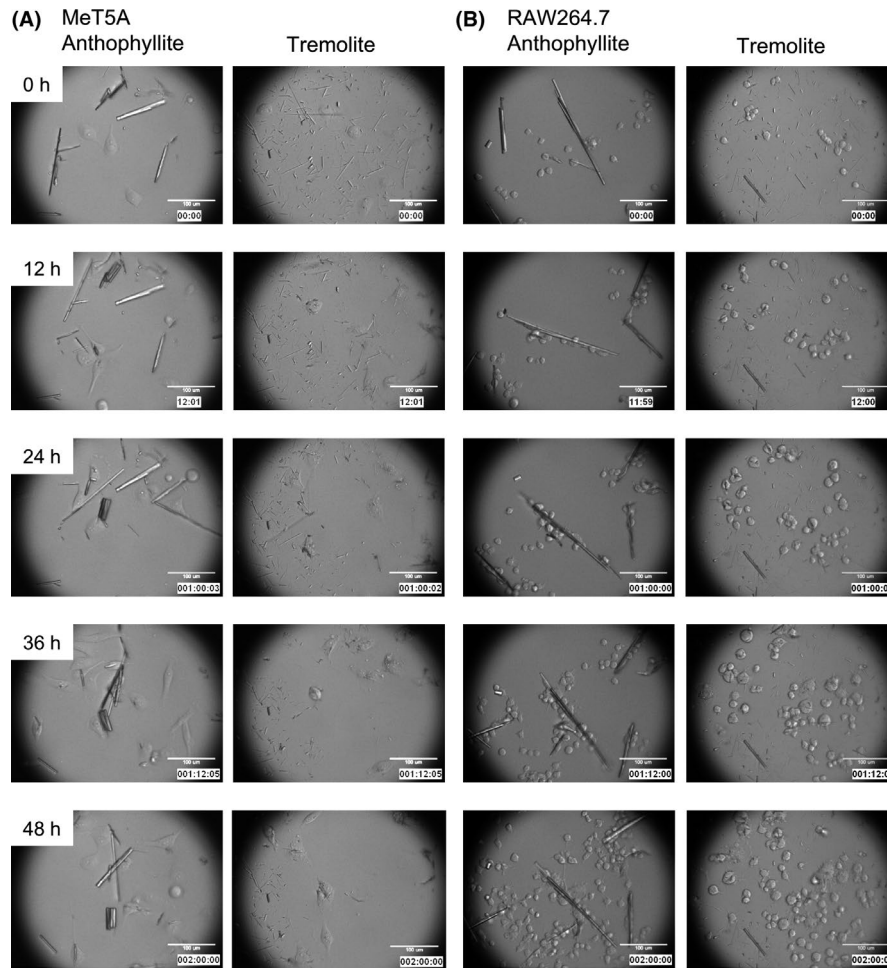


FIGURE 3 Short anthophyllite and tremolite fibers are engulfed whereas long anthophyllite fibers are attached by the pseudopod of MeT5A and RAW264.7 cells, as observed with time-lapse light microscopy. A, Long anthophyllite fibers revealed periodical swinging movement after making mechanical contact; however, a small number of short fibers were incorporated into the cytoplasm of the MeT5A cells. Tremolite was internalized from the bottom of the dish into the cytoplasm of MeT5A cells, like a cleaning floor mop. Some MeT5A cells, which were burdened with an abundance of tremolite, lost contact with the dish and disappeared from the camera, suggesting that an overload of tremolite caused MeT5A cell death (Video S1, anthophyllite; Video S2, tremolite). B, Anthophyllite that touched the cell was vibrated by the cells that aggregated around the fiber. In contrast to the cells from the epithelial or mesothelial cell lines, the RAW264.7 cells rarely swung the fibers. Tremolite was phagocytosed into Raw 264.7 cells in a manner similar to that of MeT5A cells. At 36 and 48 h, RAW264.7 cells became swollen and extended numerous protrusions explosively (Video S3, anthophyllite; Video S4, tremolite)

on days 1 and 2 but became susceptible on day 3 (Figure 4D). After incubation with tremolite for 24 hours, the release of intracellular LDH was increased significantly in the MeT5A cells but not in the RAW264.7 cells, whereas anthophyllite did not induce an increase in LDH (Figure 4E,F). The release of intracellular LDH was not significantly elevated at 24 h in HeLa, Meso8A, Meso8D, and Meso12A cell lines (Figure S5).

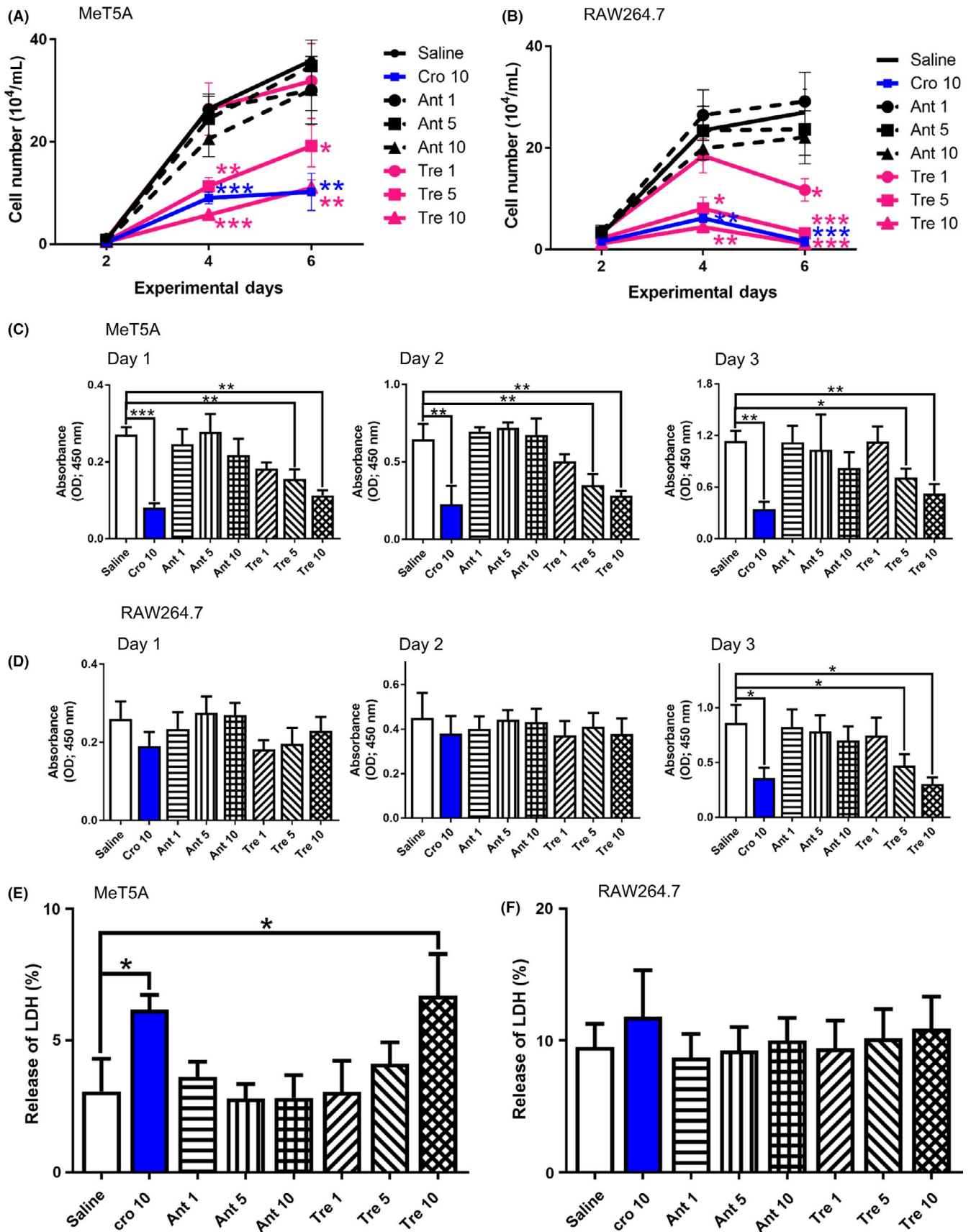
3.5 | Tremolite causes diffuse peritoneal thickening but anthophyllite generates only local fibrosis in rats

Intraperitoneal administration of tremolite induced prominent dullness of the hepatic edge 4 weeks afterwards, whereas anthophyllite induced no macroscopic changes (Figure 5A). Microscopically,

diffuse fibrous peritoneal thickening was observed in tremolite-injected rats. Anthophyllite caused granulomatous inflammation based on foreign body reaction, leading to focal fibrosis of the serosal surface in a limited manner (Figure 5). The plaque-like patchy acellular fibrosis was not observed, suggesting that plaque might not be essential for mesothelial carcinogenesis. Treatment with NTA did not affect serosal fibrosis in this experiment (Figure 5B).

3.6 | Frequent loss of *Cdkn2a/2b* in tremolite-induced MM

Whole genome scanning by aCGH detected various genomic alterations in 8 cases of rat MM induced by tremolite (Figure 6; GEO Submission GSE139106). The most frequent genomic alteration was



detected in the *Cdkn2a/2b* loci (Figure 7A). Homozygous deletion (HD) of *Cdkn2a/2b* was observed in 5 cases, and loss of heterozygosity (LOH) was observed in the remaining 3 cases. The rats that

harbored LOH of *Cdkn2a/2b* developed MM earlier than the rats that harbored HD of *Cdkn2a/2b* (Figure 7B). However, when survival was defined as either early or late by the mean survival data (282 days

FIGURE 4 Anthophyllite does not affect proliferation, whereas tremolite suppresses proliferation of MeT5A and RAW264.7 cells. A, Anthophyllite (Ant) at 1, 5, or 10 $\mu\text{g}/\text{cm}^2$ did not suppress MeT5A proliferation. Tremolite (Tre) decreased MeT5A proliferation in a dose-dependent manner. At 10 $\mu\text{g}/\text{cm}^2$, tremolite and crocidolite (Cro) induced similar levels of cytotoxicity. B, Ant at 1, 5, or 10 $\mu\text{g}/\text{cm}^2$ did not suppress RAW264.7 proliferation. Tre decreased the proliferation of RAW264.7 cells in a dose-dependent manner. At 10 $\mu\text{g}/\text{cm}^2$, Tre and Cro induced similar levels of cytotoxicity. Notably, 1 $\mu\text{g}/\text{cm}^2$ Tre significantly decreased cellular proliferation. C, Ant at 1, 5, or 10 $\mu\text{g}/\text{cm}^2$ did not suppress MeT5A proliferation, whereas Tre decreased MeT5A proliferation in a dose-dependent manner at days 1, 2, and 3. At 10 $\mu\text{g}/\text{cm}^2$, Tre and Cro caused similar levels of cytotoxicity. D, Ant did not suppress RAW264.7 proliferation. Significant suppression was observed only on day 3 for 5 and 10 $\mu\text{g}/\text{cm}^2$ Tre and for 10 $\mu\text{g}/\text{cm}^2$ Cro. E, After 24 h, release of intracellular lactate dehydrogenase (LDH) was significantly increased in MeT5A cells treated with 10 $\mu\text{g}/\text{cm}^2$ Tre or Cro. F, Release of intracellular LDH was not significantly elevated in RAW264.7 cells with every asbestos tested after 24 h (* $P < .05$, ** $P < .01$, and *** $P < .001$ vs saline)

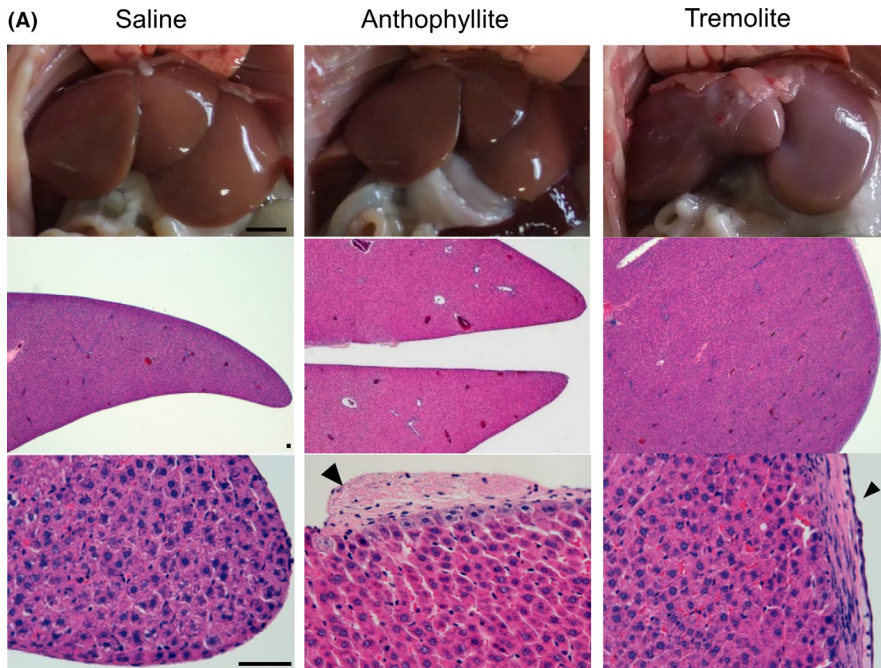
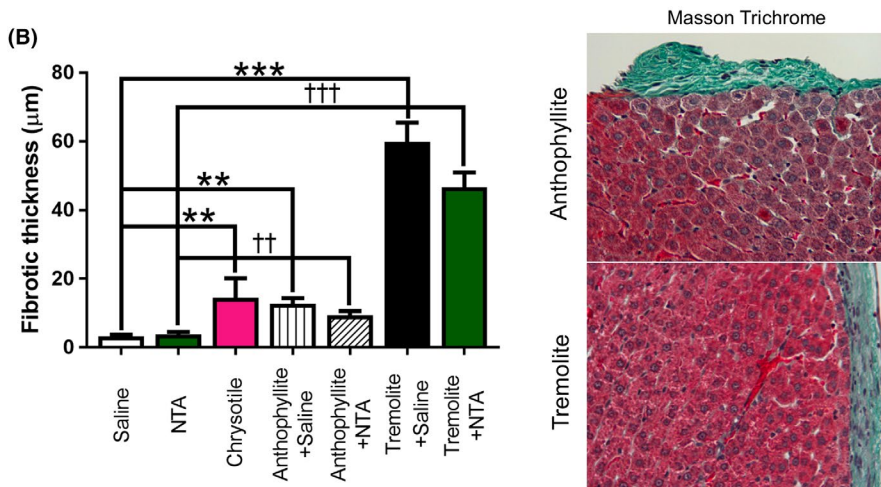


FIGURE 5 Anthophyllite induces focal fibrosis, whereas tremolite induces diffuse fibrous peritoneal thickening in rats. A, Representative images of macroscopic and microscopic photographs are shown. Anthophyllite did not induce macroscopic alteration, whereas tremolite-induced prominent dullness of hepatic edges. As highlighted by arrowheads, focal fibrosis was observed in the anthophyllite-treated rats, whereas diffuse peritoneal thickening was observed in the tremolite-treated rats (scale bar = 1 cm [photograph] and 100 μm [photomicrograph]). B, Eosinophilic fibrous tissue in H&E staining was confirmed as fibrosis by Masson's trichrome staining (** $P < .01$ and *** $P < .001$ vs saline; †† $P < .01$ and ††† $P < .001$ vs nitilotriacetate [NTA])



for tremolite and 288 days for MWCNTs), no significant correlation was observed for the relationship between early survival and LOH (Fisher's exact test; $P > .999$). Even when the data from tremolite and MWCNTs were combined to yield a mean survival of 286 days, the relationship between LOH and survival was not significant (Fisher's exact test; $P = .319$).

4 | DISCUSSION

In the present study, we observed that tremolite damages mesothelial cells and macrophages, whereas anthophyllite does not, which was in accordance with our previous finding of MM carcinogenesis.¹⁸ The long anthophyllite fibers were captured by pseudopods

FIGURE 6 Genomic loci of *Cdkn2a/2b* are the most frequently altered in tremolite-induced rat malignant mesothelioma (MM). Results of whole genome scanning are shown for 8 cases of rat MM. *Cdkn2a/2b* are the most frequently lost foci (arrowhead)

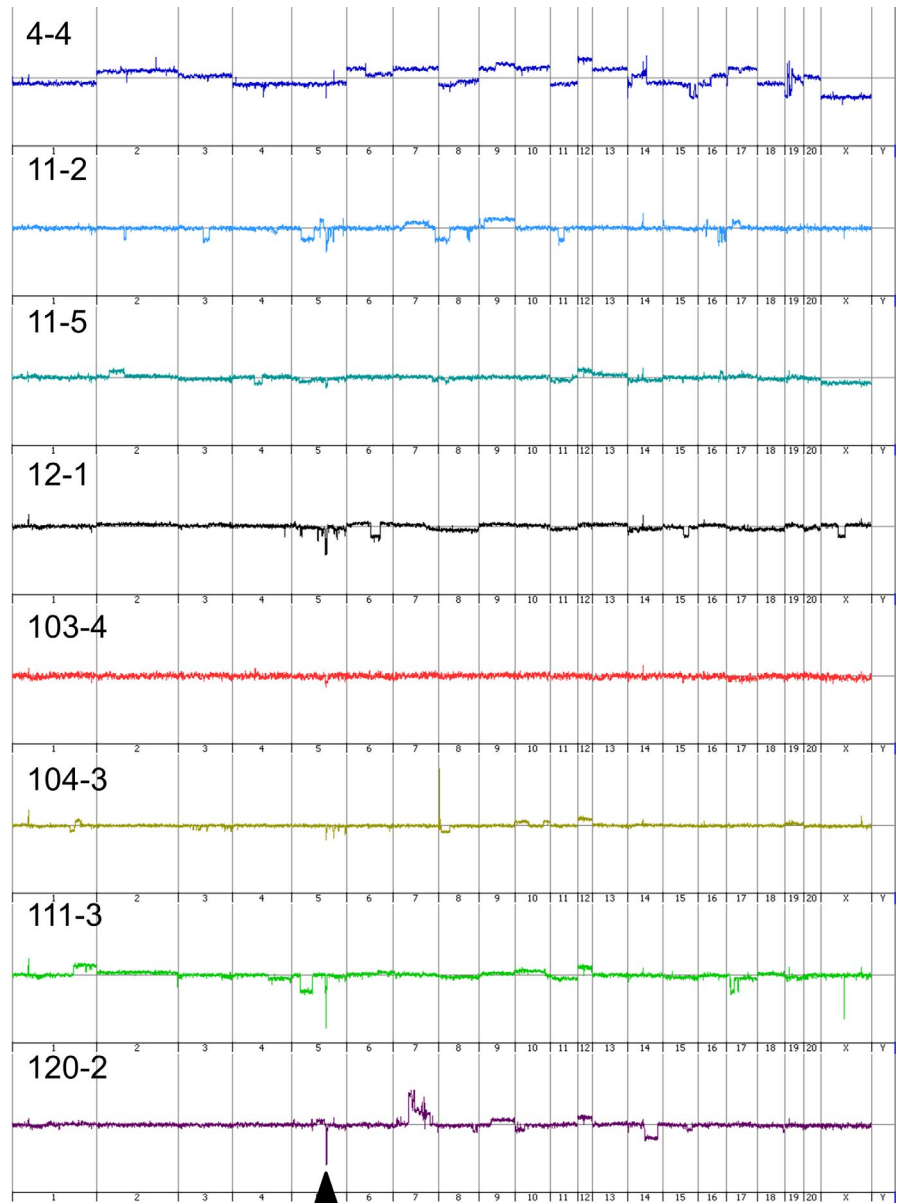


(Figure 2) and started a swinging movement after making mechanical contact (Figure 3). The long anthophyllite fibers triggered RAW264.7 cells to aggregate around the fibers, but cells from epithelial/mesothelial lineages did not aggregate, suggesting that RAW264.7 cells react aggressively to these fibers, which could be explained by the fact that RAW264.7 cells belong to immune cells. Furthermore, anthophyllite did not suppress proliferation of Met5A or RAW264.7 cells (Figure 4). Intraperitoneal injection of anthophyllite formed scattered fibrosis and granulomas in rats (Figure 5). These results are consistent with a previous study, showing that even 10 mg anthophyllite did not induce MM,¹⁸ although short anthophyllite fibers, such as those of tremolite, were phagocytosed and translocated into the cytoplasm (Figures 2 and 3).

Stanton's hypothesis states that the shapes of strongly carcinogenic fibers are 0.25 μm or less in diameter and 8 μm or more in length and that the relatively carcinogenic fibers have a diameter of 1.5 μm or less and 4 μm or longer in length.²¹ When Stanton's first definition

is used, 0% of anthophyllite and 1% of tremolite are categorized as strongly carcinogenic. When Stanton's latter definition is applied, 13% of anthophyllite and 70% of tremolite (Figure 1A) are carcinogenic, with 87% of anthophyllite, which is classified as noncarcinogenic on the basis of epidemiological evidence,¹⁰ regarded as a potent carcinogen.

In South Africa, crocidolite-induced MM was not frequently observed in the vicinity of Transvaal, whereas epidemic MM affects those in the vicinity of Cape Town.^{10,22} The diameter of the crocidolite was markedly different in the Cape Town (0.073 μm) and Transvaal (0.212 μm) samples, with similar proportions of length,¹² indicating that Stanton's hypothesis for diameter is not fully consistent with the epidemiological data. Indeed, one-half of the amphiboles found in human lungs and in mesothelioma tissues were found to be less than 5 μm in length.^{24,25} These results suggest the importance of asbestos fibers shorter than 5 μm ; thus, quantification of asbestos fibers with lengths shorter than 5 μm is proposed.^{26,27} Indeed, the partially pulverized crocidolite, 84% of which was shorter than 2.5 μm , was less

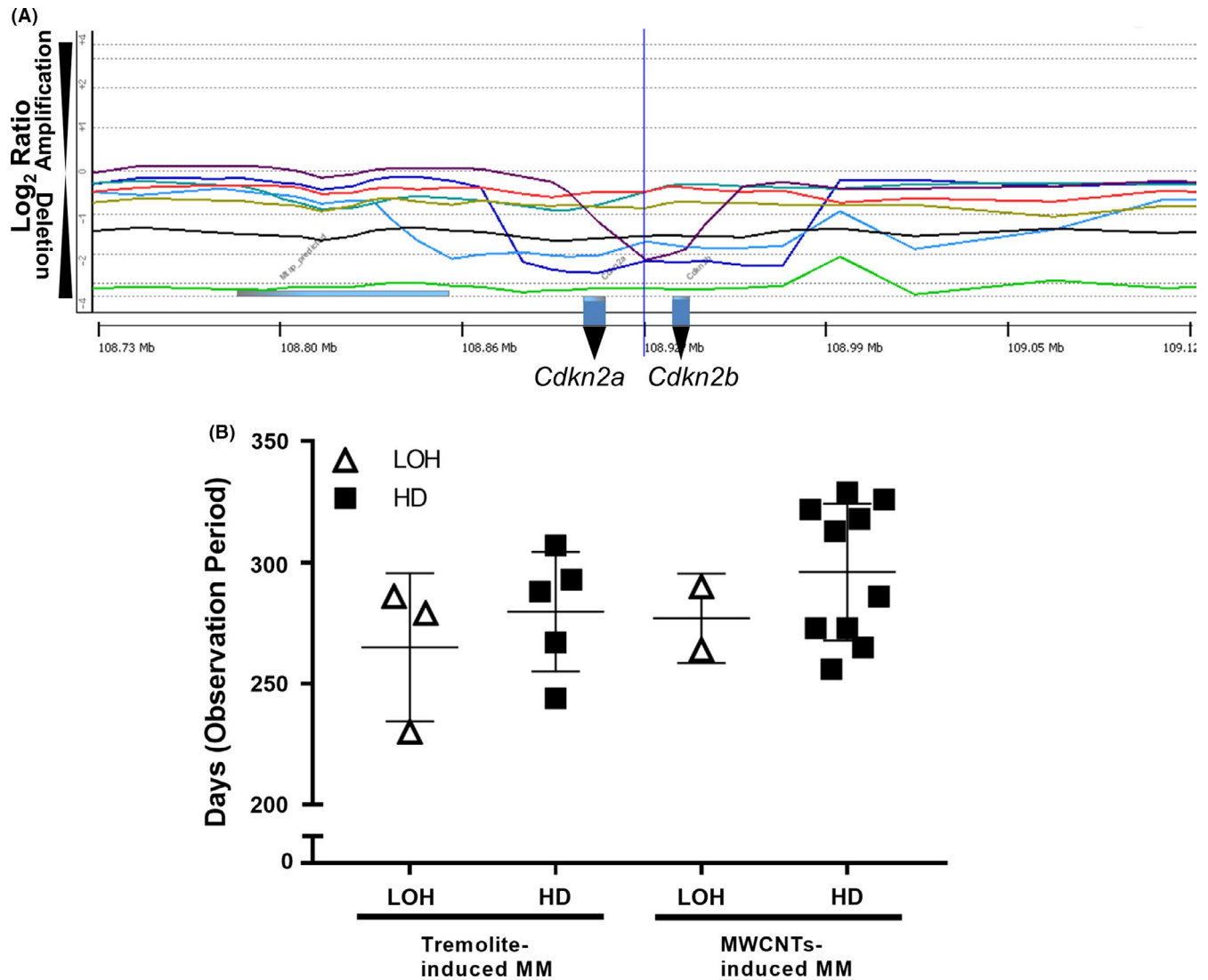


FIGURE 7 Loss of *Cdkn2a/2b* is a hallmark of tremolite-induced malignant mesothelioma (MM) in rats. A, Homozygous deletion (HD) was detected in 5 MM cases, and loss of heterozygosity (LOH) was detected in 3 MM cases. B, Relationship between genetic loss of *Cdkn2a/2b* and development of MM was analyzed for tremolite-induced together with multiwalled carbon nanotube (MWCNT)-induced rat MM to increase the number of cases. LOH of *Cdkn2a/2b* was observed earlier than HD; however, there was no significant correlation between the LOH of *Cdkn2a/2b* and the early development of MM (Fisher's exact test, $P > .999$) when the mean lifespan (282 days for tremolite and 288 days for MWCNTs) was used to define early or late onset. When the rat MM data of tremolite and MWCNT effects were combined, the mean lifespan was 286 days, and the subsequent correlation analysis between LOH and early development of MM again yielded no statistical significance (Fisher's exact test, $P = .319$)

carcinogenic than the intact crocidolite in rats.²⁸ When amosite was analyzed, the short fibers (90% of the sample fibers were shorter than 3 μm) induced MM (1/25), whereas the long fibers (30% of the sample fibers were longer than 5 μm) induced MM (20/21) in rats by i.p. injection with 25 mg amosite,²⁹ suggesting that the cut-off value for the length that induced carcinogenicity might be approximately 3 μm . Indeed, repeated intrapleural injections clearly showed that MWCNTs with lengths in the range of 0.5–2 μm and beads with diameters $3 \pm 0.1 \mu\text{m}$ did not elicit pleural inflammation; injected beads with a diameter of $10.3 \pm 0.4 \mu\text{m}$ induced inflammation in mice,³⁰ indicating that length of accurately 3 μm do not initiates mesothelial injury. For the assessment of the carcinogenicity of fibrous materials, intratracheal instillation of 1 mg each of 2 MWCNTs, with a length of $4.2 \pm 2.9 \mu\text{m}$

or $2.6 \pm 1.6 \mu\text{m}$, induced MM (3/12 and 3/12) and lung tumor (4/12 and 3/12), respectively, in F344 rats.³¹ Further, intratracheal instillation of 1.5 mg MWCNT, with a length of $4.8 \pm 2.8 \mu\text{m}$, induced a high incidence of MM (18/19) and lung tumors (1/19) in F344 rats.³² Taken together, these findings indicate that length of carcinogenic fiber might start from less than 4 μm , because Stanton's hypothesis was established on the basis of the correlation coefficients of tumor probability and the following 5 fiber length categories: 0.1–1, 1–4, 4–8, 8–64, and longer than 64 μm .²¹ Further study could reveal the characteristic property of the low carcinogenicity of anthophyllite.

In the rat model, 2 tremolite fibers, with lengths of less than 6 or 3 μm , respectively, did not induce MM in rats after intrapleural injection, whereas longer tremolite fibers induced MM.^{33,34} Furthermore,

the carcinogenicity of 10 mg tremolite that was i.p. injected completely differed by the shape of the tremolite fiber.³⁵ Even when 450 or 135 million tremolite fibers longer than 4 μm were injected i.p. into animals, the development of MM was 4/33 or 2/36, respectively.³⁵ In our previous study, 82 million tremolite fibers (1 mg) longer than 4 μm induced MM in 20 of 24 male rats and 8 of 30 female rats, whereas 820 million tremolite fibers (10 mg) induced MM in 20 of 21 male and 28 of 30 female rats.¹⁸ Furthermore, the carcinogenicities of 2 types of tremolite fibers were higher than the estimation, based on the tumor probability calculated from Stanton's hypothesis.²¹ These results indicated that a length of 4 μm might not be the clear cut-off for the carcinogenicity for tremolite. However, animal models pose the following difficulties: (i) fibers may be encapsulated in the granulomas or fibrous tissues; (ii) small fibers are deposited in the regional lymph nodes by macrophages; and (iii) formation of adhesive ileus causes death before carcinogenesis. Further study could lead to a more precise definition of the toxic biological effects of fibrous material.

Our rat model indicated that i.p. injection of iron saccharate (5 mg Fe/kg body weight) 5 days a week for 12 weeks, followed by repeated i.p. injection of NTA to promote the Fenton reaction, induced MM (17/54) in rats, which were observed for 26.7 months,³⁶ whereas i.p. injection of 1 mg MWCNT (diameter, 50 nm) induced MM in 100% of the rats within 12 months.²⁰ Furthermore, the duration of exposure to tremolite required for one-half of the rats to develop MM was 10 months;¹⁸ for crocidolite, it was 19 months.³⁷ In addition, prior to the development of lethal MM, macroscopic diffuse peritoneal thickening was observed in tremolite-injected (Figure 5) and MWCNT-injected rats²⁰; however, diffuse peritoneal thickening was less obvious, albeit present, in animals exposed to crocidolite,³⁷ chrysotile³⁸ or iron saccharate,³⁶ indicating that chronic inflammation drives the rapid development of MM. The combined effect of tremolite and NTA, an inducer of iron-induced oxidative cellular damage, was unclear (Figure 5B), thus, further study is required. The decreased production of ROS in murine neutrophils and macrophages by the overexpression of *Divalent metal transporter 1* delayed the promotional stage in crocidolite-induced mesothelial carcinogenesis,³⁹ supporting the idea that chronic inflammation-induced ROS is critical.

The early genetic event at the *Cdkn2a* locus by exposure to either long asbestos or long carbon nanotubes was the hypermethylation of *Cdkn2a*, whereas deletion of *Cdkn2a* occurs at a late stage of the malignant transformation.⁴⁰ The homozygous deletion of *Cdkn2a/2b* was not observed in the epithelioid subtype (EM) (0/6), but it was observed in the sarcomatoid subtype (SM) (4/5) in our study³⁶ and EM (1/5) in another study⁴¹ when iron saccharate was used for rat MM carcinogenesis. The higher rate of homozygous deletion of *Cdkn2a/2b* in SM is concordant with human MM.⁴² Here, the coexistence of homozygous (5/8) or hemizygous deletions (3/8) of *Cdkn2a/2b* loci were observed in the cases of tremolite-induced MM (Figure 7A), as they were after MWCNT injections,²⁰ whereas the majority of the genetic disruption to *Cdkn2a/2b* was homozygous deletion by crocidolite (8/9), amosite (9/9), and chrysotile (8/9).³⁸ These biodurable fibers are presumed to be entangled with chromosomes³; however, the mechanism by which *Cdkn2a/2b* loci are preferentially damaged

remains unclear. The early development of MM was implicated with lower rates of homozygous deletion of *Cdkn2a/2b* (Figure 7B); however, the relationship between the early development of MM and LOH was not statistically significant in our model. These results could suggest that chronic inflammation accelerates the fibrosis and development of MM through a positive feedback loop through cytokines, such as connective tissue growth factor^{43,44} and/or transforming growth factor- β ⁴⁵ without deletion of *Cdkn2a/2b*.

In conclusion, anthophyllite did not evoke mesothelial injury, whereas tremolite caused cytotoxicity to the mesothelial cells and macrophages, leading to chronic inflammation and mesothelial carcinogenesis. Here again the major target gene was homozygous deletion of *Cdkn2a/2b*.

ACKNOWLEDGMENTS

We thank Mr Koji Itakura (Nagoya University, Graduate School of Medicine, Division of Molecular Research Engineering) for his excellent instruction on operating an electron microscope (JSM-7610F and JEM-1400 PLUS) and Dr Akihiro Sakai (Nagoya University, Medical School) for his technical assistance. This work was supported, in part, by a JSPS Kakenhi grant (JP25860292) to YO, and a JSPS Kakenhi grants (JP17H04064 and JP19H05462) and Private University Research Branding Project to ST.

DISCLOSURE

Authors declare no conflicts of interest.

ORCID

Yasumasa Okazaki  <https://orcid.org/0000-0003-1054-9403>
Shinya Toyokuni  <https://orcid.org/0000-0002-5757-1109>

REFERENCES

1. Furuya S, Chimed-Ochir O, Takahashi K, David A, Takala J. Global asbestos disaster. *Int J Environ Res Public Health*. 2018;15:1000.
2. Holmes D. IARC in the dock over ties with asbestos industry. *Lancet*. 2013;381:359-361.
3. Toyokuni S. Iron addiction with ferroptosis-resistance in asbestos-induced mesothelial carcinogenesis: toward the era of mesothelioma prevention. *Free Radic Biol Med*. 2019;133:206-215.
4. IARC Working Group on the Evaluation of Carcinogenic Risks to Humans. Arsenic, metals, fibres, and dusts. *IARC Monogr Eval Carcinog Risks Hum*. 2012;100:11-465.
5. Finkelstein MM. Malignant mesothelioma incidence among talc miners and millers in New York State. *Am J Ind Med*. 2012;55:863-868.
6. Garabrant DH, Pastula ST. A comparison of asbestos fiber potency and elongate mineral particle (EMP) potency for mesothelioma in humans. *Toxicol Appl Pharmacol*. 2018;361:127-136.
7. Tuomi T. Fibrous minerals in the lungs of mesothelioma patients: comparison between data on SEM, TEM, and personal interview information. *Am J Ind Med*. 1992;21:155-162.
8. Hiraoka T, Ohkura M, Morinaga K, Kohyama N, Shimazu K, Ando M. Anthophyllite exposure and endemic pleural plaques in Kumamoto, Japan. *Scand J Work Environ Health*. 1998;24:392-397.
9. Gaffney SH, Grespin M, Garnick L, et al. Anthophyllite asbestos: state of the science review. *J Appl Toxicol*. 2017;37:38-49.
10. Harington JS. Fiber carcinogenesis: epidemiologic observations and the Stanton hypothesis. *J Natl Cancer Inst*. 1981;67:977-989.

11. Karjalainen A, Meurman LO, Pukkala E. Four cases of mesothelioma among Finnish anthophyllite miners. *Occup Environ Med.* 1994;51:212-215.
12. Gualtieri AF, Pollastri S, Bursi Gandolfi N, Gualtieri ML. In vitro acellular dissolution of mineral fibres: a comparative study. *Sci Rep.* 2018;8:7071.
13. McDonald JC, McDonald AD, Hughes JM. Chrysotile, tremolite and fibrogenicity. *Ann Occup Hyg.* 1999;43:439-442.
14. Kohyama N, Fujiki M, Kishimoto T, Morinaga K. Lung cancer in a patient with predominantly short tremolite fibers in his lung. *Am J Ind Med.* 2017;60:831-838.
15. Donaldson K, Murphy FA, Duffin R, Poland CA. Asbestos, carbon nanotubes and the pleural mesothelium: a review of the hypothesis regarding the role of long fibre retention in the parietal pleura, inflammation and mesothelioma. *Part Fibre Toxicol.* 2010;7:5.
16. Toyokuni S. The origin and future of oxidative stress pathology: from the recognition of carcinogenesis as an iron addiction with ferroptosis-resistance to non-thermal plasma therapy. *Pathol Int.* 2016;66:245-259.
17. Kohyama N, Shinohara Y, Suzuki Y. Mineral phases and some re-examined characteristics of the International Union Against Cancer standard asbestos samples. *Am J Ind Med.* 1996;30:515-528.
18. Aierken D, Okazaki Y, Chew SH, et al. Rat model demonstrates a high risk of tremolite but a low risk of anthophyllite for mesothelial carcinogenesis. *Nagoya J Med Sci.* 2014;76:149-160.
19. Usami N, Fukui T, Kondo M, et al. Establishment and characterization of four malignant pleural mesothelioma cell lines from Japanese patients. *Cancer Sci.* 2006;97:387-394.
20. Nagai H, Okazaki Y, Chew SH, et al. Diameter and rigidity of multiwalled carbon nanotubes are critical factors in mesothelial injury and carcinogenesis. *Proc Natl Acad Sci USA.* 2011;108:E1330-1338.
21. Stanton MF, Layard M, Tegeris A, et al. Relation of particle dimension to carcinogenicity in amphibole asbestoses and other fibrous minerals. *J Natl Cancer Inst.* 1981;67:965-975.
22. Rees D, Myers JE, Goodman K, et al. Case-control study of mesothelioma in South Africa. *Am J Ind Med.* 1999;35:213-222.
23. Timbrell V, Griffiths DM, Pooley FD. Possible biological importance of fibre diameters of South African amphiboles. *Nature.* 1971;232:55-56.
24. Dodson RF, Atkinson MA, Levin JL. Asbestos fiber length as related to potential pathogenicity: a critical review. *Am J Ind Med.* 2003;44:291-297.
25. Suzuki Y, Yuen SR, Ashley R. Short, thin asbestos fibers contribute to the development of human malignant mesothelioma: pathological evidence. *Int J Hyg Environ Health.* 2005;208:201-210.
26. Bernstein DM, Kunzendorf P. Standardized methods for preparation and bi-variate length & diameter counting/sizing of aerosol and tissue digestion fiber samples. *Toxicol Appl Pharmacol.* 2018;361:174-184.
27. Boulanger G, Andujar P, Pairon JC, et al. Quantification of short and long asbestos fibers to assess asbestos exposure: a review of fiber size toxicity. *Environ Health.* 2014;13:59.
28. Stanton MF, Wrench C. Mechanisms of mesothelioma induction with asbestos and fibrous glass. *J Natl Cancer Inst.* 1972;48:797-821.
29. Davis JM, Addison J, Bolton RE, Donaldson K, Jones AD, Smith T. The pathogenicity of long versus short fibre samples of amosite asbestos administered to rats by inhalation and intraperitoneal injection. *Br J Exp Pathol.* 1986;67:415-430.
30. Murphy FA, Poland CA, Duffin R, et al. Length-dependent retention of carbon nanotubes in the pleural space of mice initiates sustained inflammation and progressive fibrosis on the parietal pleura. *Am J Pathol.* 2011;178:2587-2600.
31. Suzui M, Futakuchi M, Fukamachi K, et al. Multiwalled carbon nanotubes intratracheally instilled into the rat lung induce development of pleural malignant mesothelioma and lung tumors. *Cancer Sci.* 2016;107:924-935.
32. Numano T, Higuchi H, Alexander DB, et al. MWCNT-7 administered to the lung by intratracheal instillation induces development of pleural mesothelioma in F344 rats. *Cancer Sci.* 2019;110:2485-2492.
33. Wagner JC. Mesothelioma and mineral fibers. *Cancer.* 1986;57:1905-1911.
34. Wagner JC, Chamberlain M, Brown RC, et al. Biological effects of tremolite. *Br J Cancer.* 1982;45:352-360.
35. Davis JM, Addison J, McIntosh C, Miller BG, Niven K. Variations in the carcinogenicity of tremolite dust samples of differing morphology. *Ann N Y Acad Sci.* 1991;643:473-490.
36. Hu Q, Akatsuka S, Yamashita Y, et al. Homozygous deletion of CDKN2A/2B is a hallmark of iron-induced high-grade rat mesothelioma. *Lab Invest.* 2010;90:360-373.
37. Nagai H, Okazaki Y, Chew SH, Misawa N, Yasui H, Toyokuni S. Deferasirox induces mesenchymal-epithelial transition in crocidolite-induced mesothelial carcinogenesis in rats. *Cancer Prev Res (Phila).* 2013;6:1222-1230.
38. Jiang L, Akatsuka S, Nagai H, et al. Iron overload signature in chrysotile-induced malignant mesothelioma. *J Pathol.* 2012;228:366-377.
39. Funahashi S, Okazaki Y, Nishiyama T, et al. Global overexpression of divalent metal transporter 1 delays crocidolite-induced mesothelial carcinogenesis in male mice. *Free Radic Res.* 2018;52:1030-1039.
40. Chernova T, Murphy FA, Galavotti S, et al. Long-fiber carbon nanotubes replicate asbestos-induced mesothelioma with disruption of the tumor suppressor gene Cdkn2a (Ink4a/Arf). *Curr Biol.* 2017;27:3302-3314.e6.
41. Minami D, Takigawa N, Kato Y, et al. Downregulation of TBXAS1 in an iron-induced malignant mesothelioma model. *Cancer Sci.* 2015;106:1296-1302.
42. Illei PB, Rusch VW, Zakowski MF, Ladanyi M. Homozygous deletion of CDKN2A and codeletion of the methylthioadenosine phosphorylase gene in the majority of pleural mesotheliomas. *Clin Cancer Res.* 2003;9:2108-2113.
43. Jiang L, Yamashita Y, Chew SH, et al. Connective tissue growth factor and beta-catenin constitute an autocrine loop for activation in rat sarcomatoid mesothelioma. *J Pathol.* 2014;233:402-414.
44. Ohara Y, Chew SH, Misawa N, et al. Connective tissue growth factor-specific monoclonal antibody inhibits growth of malignant mesothelioma in an orthotopic mouse model. *Oncotarget.* 2018;9:18494-18509.
45. Fujii M, Toyoda T, Nakanishi H, et al. TGF-beta synergizes with defects in the Hippo pathway to stimulate human malignant mesothelioma growth. *J Exp Med.* 2012;209:479-494.

SUPPORTING INFORMATION

Additional supporting information may be found online in the Supporting Information section.

How to cite this article: Okazaki Y, Misawa N, Akatsuka S, et al. Frequent homozygous deletion of *Cdkn2a/2b* in tremolite-induced malignant mesothelioma in rats. *Cancer Sci.* 2020;111:1180-1192. <https://doi.org/10.1111/cas.14358>